Using Inertial Fusion Implosions to Measure the T+^{3}He Fusion Cross Section at Nucleosynthesis-Relevant Energies

A. B. Zylstra, H. W. Herrmann, M. Gatu Johnson, Y. H. Kim, J. A. Frenje, G. Hale, C. K. Li, M. Rubery, M. Paris, A. Bacher, C. R. Brune, C. Forrest, V. Yu. Glebov, R. Janezic, D. McNabb, A. Nikroo, J. Pino, T. C. Sangster, F. H. Séguin, W. Seka, H. Sio, C. Stoeckl, and R. D. Petrasso

Phys. Rev. Lett. **117**, 035002 — Published 11 July 2016

DOI: 10.1103/PhysRevLett.117.035002

Using inertial fusion implosions to measure the T+^{3}He fusion cross section at nucleosynthesis-relevant energies

A. B. Zylstra,[1,2,*] H. W. Herrmann,[2] M. Gatu Johnson,[1] Y. H. Kim,[2] J. A. Frenje,[1] G. Hale,[2] C. K. Li,[1] M. Rubery,[3] M. Paris,[2] A. Bacher,[4] C. R. Brune,[5] C. Forrest,[6] V. Glebov,[6] R. Janezic,[6] D. McNabb,[7] A. Nikroo,[8] J. Pino,[7] T. C. Sangster,[6] F. H. Séguin,[1] W. Seka,[6] H. Sio,[1] C. Stoeckl,[6] and R. D. Petrasso[1]

[1] *Plasma Science and Fusion Center, Massachusetts Institute of Technology, Cambridge, Massachusetts 02139, USA*
[2] *Los Alamos National Laboratory, Los Alamos, New Mexico 87545, USA*
[3] *Plasma Physics Department, AWE plc, Reading RG7 4PR, United Kingdom*
[4] *Indiana University, Bloomington, Indiana 47405, USA*
[5] *Ohio University, Athens, Ohio 45701, USA*
[6] *Laboratory for Laser Energetics, University of Rochester, Rochester, New York 14623, USA*
[7] *Lawrence Livermore National Laboratory, Livermore, California 94550, USA*
[8] *General Atomics, San Diego, California 92186, USA*

Light nuclei were created during big-bang nucleosynthesis (BBN). Standard BBN theory, using rates inferred from accelerator-beam data, cannot explain high levels of ^{6}Li in low-metallicity stars. Using high-energy-density plasmas we measure the T(^{3}He,γ)^{6}Li reaction rate, a candidate for anomalously-high ^{6}Li production; we find that the rate is too low to explain the observations, and different than values used in common BBN models. This is the first data directly relevant to BBN, and also the first use of laboratory plasmas, at comparable conditions to astrophysical systems, to address a problem in nuclear astrophysics.

PACS numbers: 52.57.-z, 26.35.+c, 98.80.Ft

While most light nuclei abundances in primordial material are explained well by big-bang nucleosynthesis (BBN) theory[1–3], observations of high levels of ^{6}Li in low-metallicity stars[4, 5] disagree with BBN models by three orders of magnitude. During BBN several nuclear reactions could produce excess ^{6}Li, in particular ^{4}He(D,γ)^{6}Li and ^{3}He(T,γ)^{6}Li. Recent work has ruled out the first reaction[6], while the latter has been hypothesized as a solution to this problem[7], if the rate is much higher than expected, or in non-standard production models.

The nuclear physics of the ^{3}He(T,γ)^{6}Li reaction explaining these astrophysical observations is contentious[8] yet still an open question[3]. This is primarily due to the lack of high-quality data for this reaction, with previous experiments being conducted at high energies and with significant inconsistencies between the reported datasets[9]. Only one dataset exists at low energy ($E_{cm} \leq 1$ MeV)[9], which is still higher than the range where BBN reactions occurred; the fidelity of this data has also been questioned in the literature[3, 7]. This strongly motivates additional experiments to determine if this reaction could explain the observed levels of ^{6}Li in low-metallicity stars via BBN production.

In this Letter we report on novel measurements of the T(^{3}He,γ)^{6}Li reaction using high-energy-density plasmas (HEDP), which were generated by using the OMEGA laser facility[10] to implode gas-filled thin-glass 'exploding pusher'[11] capsules. In these experiments, the laser delivered 17kJ of energy in a 600ps duration square pulse, illuminating the outer surface of a glass microballoon 960 μm in diameter and 2.5 μm thick, filled with T_2 and ^{3}He gas with a total pressure of 20 atm and a 30:70 atomic mixture. Capsules filled with T_2, ^{3}He, or a D_2+^{3}He mixture were used for background measurements and instrument calibration. Ablation pressures on the order of tens of MBar rapidly developed as the laser energy was absorbed in the glass shell's outer surface, launching a strong spherically-converging shock into the gas. When this shock reached the center of the capsule and rebounded, it created a high-temperature and high-density plasma in which nuclear reactions occurred[11]. In these implosions, ion temperatures reached ~ 20 keV (2.3×10^8 K) while ion number densities were $\sim 4\times10^{22}$ cm^{-3}, and fusion burn occurred over ~ 100 ps.

The T(^{3}He,γ)^{6}Li reaction produces an energetic γ ray at 15.8 MeV, which was measured with a Gas Cherenkov Detector (GCD)[12]. In this instrument, the incident γ rays Compton scatter electrons from a converter foil into a gas-filled pressure cell, where the electrons exceed the local speed of light, producing Cherenkov light that is detected with a photomultiplier tube[12, 13]. The number of detected Cherenkov photons depends on the detector response and total number of γ rays produced in the implosion. The detector response depends on the geometry, γ-ray energy, and index of refraction of the cell gas (determined by the gas type and density). This experiment used CO_2 gas at 100psi. The detector response is calculated using GEANT4[14] and calibrated in-situ using D^{3}He γs[13]. The PMT signal is recorded on an oscilloscope and background-subtracted using regions before and after the signal peak.

The raw Cherenkov detector data are shown in Fig. 1. Each curve corresponds to a single implosion on the left,

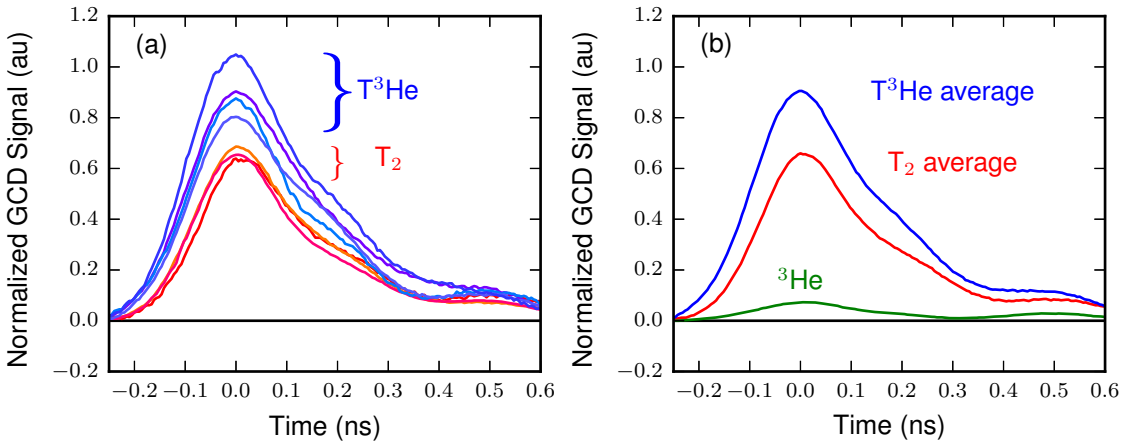

FIG. 1: Left: Cherenkov data from individual implosions with T^3He or T_2 fuel; right: Average and yield-normalized data for each fuel type. $t = 0$ occurs at the signal peak for each curve. In addition to the T^3He-gas-filled implosions (blue), sources of background are measured with T_2 (red) or ^3He gas-filled (green) implosions. The T_2 and T^3He implosions are normalized by the measured DT-neutron yield produced in each shot.

which are averaged by fuel type on the right. The peak signal corresponds to the peak γ production, with each curve shifted so peak burn occurs at $t = 0$. The signal width corresponds to a combination of the instrument temporal response and the burn duration of the implosion. The signal later in time at ~ 0.5 ns is a photomultiplier tube 'ring', due to a slight impedance mismatch. The data from the T^3He-filled implosions are shown by the blue curves.

The total integrated signal (V×s) is

$$\mathrm{V}\times\mathrm{s} = Y_\gamma \times \Omega \times \Big(\chi \times R_{p/\gamma}\Big) \times \Big[\mathrm{QE}\times G \times e \times R_t\Big]. \quad (1)$$

In Eq. 1, Y_γ is the total γ-ray yield and Ω is the detector solid angle (1.10×10^{-2}). The quantity in parentheses is the detector response: χ is the calibration factor, and $R_{p/\gamma}$ is the number of detected Cherenkov photons per incident γ. The latter quantity depends on the incident γ energy. The detector calibration factor is primarily due to uncertainty in the calculated light collection and is found to be $\chi = 0.65$ (Ref. 13). The quantity in square brackets is the electrical response of the system: the PMT quantum efficiency (QE) and gain (G), the fundamental charge (e), and termination resistance ($R_t = 50\ \Omega$). A Photek 210 PMT was used with a Cherenkov-spectrum ($1/\lambda^2$) weighted effective QE of 8.4% and gain of 1.46×10^6. Fig. 2 shows the calculated response, using GEANT4[14], for the Cherenkov instrument under these conditions: the number of productive electrons and Cherenkov photons detected per incident γ (blue and blue dashed curves, left axis) as well as the number of Cherenkov photons detected per electron (red, right axis).

Since V×s is the measured quantity (given in Supplemental Table 1), Eq. 1 can be inverted to obtain the γ yield, number of Compton electrons ($N_e = Y_\gamma \times \Omega \times R_{e/\gamma}$), and number of Cherenkov photons ($N_p = Y_\gamma \times \Omega \times R_{p/\gamma}$). Since each Compton electron generates multiple detected Cherenkov photons (see Fig. 2), N_e is used in our statistical analysis and uncertainties.

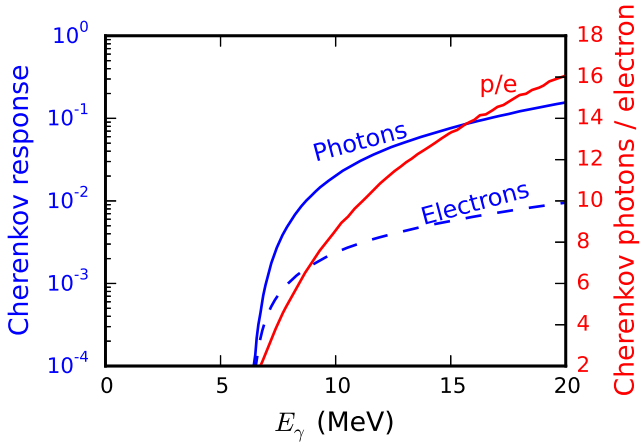

FIG. 2: Cherenkov detector response (100psi CO_2) from a GEANT4 calculation. Left: productive electrons and Cherenkov photons detected per incident γ (blue and blue dashed curves, respectively). Right: the number of photons detected per productive electron (red curve).

Background for this measurement includes nuclear and plasma sources. Nuclear sources are other nuclear reactions that also produce γ rays detected by the GCD. Plasma sources are high-energy photons produced by laser-plasma interactions or bremsstrahlung radiation

that are energetic enough to produce Cherenkov light in the gas cell, or that directly interact with the PMT.

There are three main sources of background in the measured $V \times s$. The primary source is due to a $\sim 1.5\%$ deuterium (D) impurity in the T_2 gas used for these experiments, resulting in D+T reactions that generate γ rays at 16.75 MeV with a branching ratio of $\sim 4 \times 10^{-5}$ (fraction of total DT reactions)[13]. With a 1.5% D contamination level and the significantly higher D+T fusion cross section, this is the dominant source of background. T_2-filled implosions with the same D contamination were used to measure the background level, shown as red curves in Fig. 1. On the T_2 shots, the total Cherenkov signal and DT neutron yield were measured, the latter with standard time-of-flight diagnostics[15], giving the Cherenkov signal produced per DT neutron. Since the DT γ/n ratio is constant between shots in this experiment, this factor is used with the measured DT neutron yield (Supplemental Table 2) to calculate the Cherenkov signal due to DT reactions in the T^3He implosions. There is a $\sim 5\%$ statistical uncertainty in this subtraction due to the neutron yield measurement and number of Compton electrons scattered by DT-γs.

A second source of background was observed in an implosion with only ^{3}He gas, shown in Fig. 1 by the green curve; this background is due to either a plasma or nuclear process [13]. When scaling to the T^3He data shots, this source of background is expected to be either constant (if a plasma process) or scale with the ^{3}He number density squared if a nuclear process. These are taken as upper and lower limits, respectively, because of the uncertain nature of this background and thus contribute to the final systematic uncertainty.

A third source of background is D^3He reactions, producing γ rays with a γ/p branching ratio of $\sim 1.2 \times 10^{-4}$ (Ref. 16). The contribution from D^3He fusion is subtracted using D^3He proton yields, which were measured using proton spectrometry[17] (see Supplemental Table 2). The yield is combined with the detector response and γ/proton branching ratio[16] to infer the signal due to D^3He-γs, which has a statistical uncertainty due to the D^3He-p measurement and Compton electron statistics, plus a systematic uncertainty due to the branching ratio.

The T^3He γ contribution to the total signal ($V \times s$ given in Supplemental Table 1) is determined by subtracting the three background sources. To calculate the γ-ray yield, the effective detector response to T^3He γs is needed, which depends on their spectrum. In the capture reaction, the ^{6}Li can be produced in either the ground state or an excited state, which affects the produced γ-ray spectrum. The T^3He γ-ray spectrum was calculated using R-matrix nuclear theory (see Supplemental Information), which is shown in Fig. 3 (blue curve). While the largest component in the spectrum is the ground state contribution (γ_0, $E_\gamma \sim 15.8$ MeV), capture to excited states of ^{6}Li, at lower γ-ray energies, is significant.

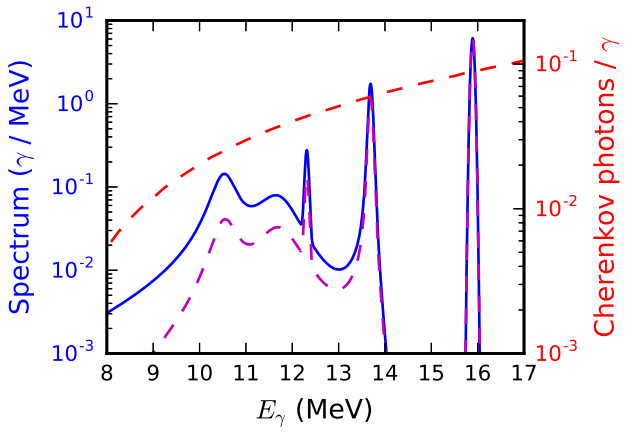

FIG. 3: Calculated γ-ray spectrum (blue, area normalized), detector response (red), and spectrum normalized to sensitivity (magenta).

If all of the reactions proceeded to the ground state, the detector sensitivity would be $R_{p/\gamma} = 8.75 \times 10^{-2}$ and $R_{e/\gamma} = 6.30 \times 10^{-3}$. The prior work by Blatt et al. (Ref. 9) gives cross-sections for γ_0, γ_1, and γ_2 at $E_{cm} = 250$ keV; if these branching ratios are used with the mean γ energies, the detector's effective sensitivity is then $R_{p/\gamma} = (7.7 \pm 1.0) \times 10^{-2}$ and $R_{e/\gamma} = (5.7 \pm 0.7) \times 10^{-3}$. Using the R-matrix calculated spectrum, the detector's effective sensitivity is $R_{p/\gamma} = 6.91 \times 10^{-2}$ and $R_{e/\gamma} = 5.27 \times 10^{-3}$, or a reduction of $\sim 20\%$ in sensitivity compared to the case where all reactions capture to the ground state (γ_0). The sensitivity using Blatt's published data is consistent with the calculated R-matrix spectrum. The R-matrix spectrum weighted by the detector response is the dashed magenta curve in Fig. 3, showing the suppression of the excited state contribution to the total signal.

With this methodology, the calculated γ-ray yield and reaction S-factor are for all channels: capture to the ground state and all excited states of ^{6}Li. In astrophysical work, the quantity of interest is the cross section for production of ^{6}Li, and thus includes capture to the ground state and second excited state (which decays via γ emission) but not the first or higher excited states (in which the ^{6}Li breaks up in the decay). Using the detector sensitivity in the previous paragraph gives a total γ yield (or total S-factor). The S-factor for astrophysical production of ^{6}Li, denoted S_a, is smaller by a factor of 0.58 according to our R-matrix calculation. This value is also consistent with the Blatt data (the only accelerator-beam experiment below 1 MeV center-of-mass energy).

With these effective sensitivities, the total γ-ray yield (Y_γ) is calculated using Eq. 1. An additional statistical uncertainty is included in Y_γ as $1/\sqrt{N_e}$ where N_e is the number of Compton electrons corresponding to the

T^3He signal, and an additional 33.4% absolute calibration uncertainty[13] in χ is added to the systematic uncertainty. The quantity of interest in these experiments is the astrophysical S-factor (S) for the $T(^3He,\gamma)^6Li$ reaction, which is related to the cross section (σ) as

$$\sigma(E_{cm}) = S(E_{cm})\frac{e^{-\sqrt{E_G/E_{cm}}}}{E_{cm}}, \quad (2)$$

where E_{cm} is the center-of-mass energy for the fusion reaction and E_G is the Gamow energy, which is a constant. The S-factor is only weakly dependent on E_{cm}. The center-of-mass energy ($E_{cm} = 81\pm6$ keV) for the reaction is determined from the Doppler spread of D^3He protons. In a thermal plasma, the center-of-mass energies of occurring reactions are determined by the product of the cross section and the reactant distribution (Maxwellian). The average center-of-mass energy is often referred to as the Gamow peak energy. From the line width of the D^3He-proton spectrum, a thermal Maxwellian ion temperature (T_i) was determined from the proton Doppler spread[18] (see Supplemental Table 2). Radiation-hydrodynamic simulations show that the T^3He and D^3He reactions have burn-averaged temperatures well within 1 keV due to the similar reactivity energy dependence, suggesting a similar T_i for the T^3He reaction. To account for the reliance on simulation, we increase the uncertainty by ±1 keV for the T^3He reaction. The measurements from individual shots are used when calculating a S-factor for that shot.

To determine the S-factor from the γ yield in this experiment, a better-known T^3He reaction branch is used as a reference: $T(^3He,D)^4He$. The absolute yield of the 9.5 MeV deuterons was measured on each shot with six independent detectors using two different techniques: direct CR-39 track detection[17] and dipole magnetic spectroscopy[17, 19]. The data are shown in Supplemental Table 2. The deuteron yield measurement has a $\sim 1\%$ statistical and $\sim 3\%$ systematic uncertainty.

The S-factor is then calculated for each shot as $S_\gamma = S_D \times Y_\gamma/Y_d$. The deuteron branch S-factor ($S_d = 568$ keV-b) was taken from ENDF[20] with a 5% uncertainty[21]. To reduce statistical uncertainties a weighted mean of the shots is taken, statistically weighted using the number of Compton electrons generated by T^3He-γs. We find that the total S-factor for the $T(^3He,\gamma)^6Li$ branch is

$$S_\gamma = 0.35 \pm 0.05_{\rm stat} \pm 0.14_{\rm sys} \ \ \text{keV-b}. \quad (3)$$

Uncertainty due to the T_i uncertainty is propagated when calculating S_γ. The values for each shot are shown in Supplemental Table 1. The astrophysical S-factor ($S_{\gamma,a}$) for production of ^6Li is smaller by a factor of $0.58\times$, giving

$$S_{\gamma,a} = 0.20 \pm 0.03_{\rm stat} \pm 0.07_{\rm sys} \ \ \text{keV-b}. \quad (4)$$

Gradients in plasma conditions, which occur in these implosions, do not affect this measurement. Since the ratio is taken to another branch of the $T+^3He$ reaction, density gradients cannot affect the data as both reactions have the same reactants. Temperature gradients can cause the measurement to sample a range of center-of-mass energies. A signature of this is additional kurtosis in monoenergetic fusion spectra[22]; analysis of the D^3He proton data shows kurtosis $0.1-0.3$ corresponding to $\delta T/T \lesssim 0.1$, comparable to the T_i uncertainty.

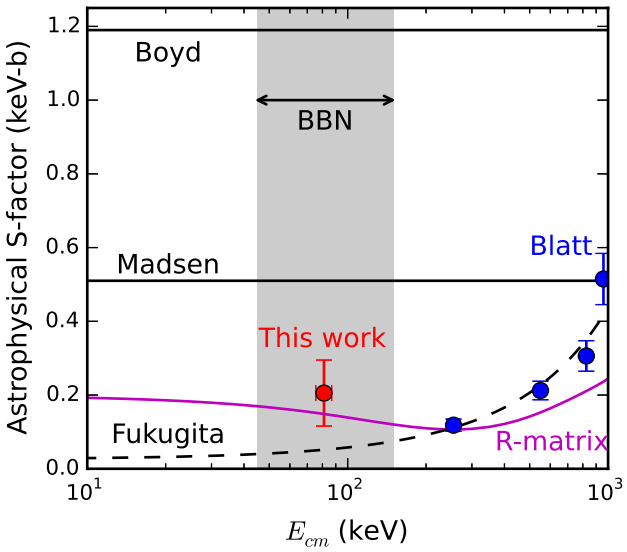

FIG. 4: Astrophysical S-factor for the reaction $T(^3He,\gamma)^6Li$ measured in this work, compared to previous data[9] and constant values used in BBN theory[3, 7]. The total uncertainty for this measurement (statistical and systematic) is shown. The energy range of interest to BBN, $45-150$ keV, is shown by the shaded region.

The astrophysical S-factor determined in this work is shown in Fig. 4 with a total uncertainty (quadrature sum of statistical and systematic), and contrasted to higher-energy data obtained in previous experimental work by Blatt[9]. The energy range relevant to standard BBN is $45-150$ keV[23]; this work is the first measurement in the applicable energy range. Values used in BBN reaction theories[3, 7, 8] are also shown for comparison. Finally, a R-matrix calculation fit to the higher-energy accelerator data from Blatt, is shown in the magenta curve. Our data shows good agreement with the R-matrix calculation, which was fit to 90° differential cross section data. The difference in the astrophysical S-factor between our R-matrix calculation and the Blatt results at $500-1000$ keV is due to a discrepancy in the angular distribution, as the Blatt data were measured at 90° but our data are over 4π. Astrophysical calculations need the 4π value. The S-factor's rise at low energy is due to resonance in

^{6}Li (see Supplemental Fig. 1) that was not included in previously reported ^{6}Li energy levels[24].

Among the BBN models, the S-factor used by Boyd[3] is a significant overestimate of the reaction rate at $E_{cm} \leq$ 1 MeV; Madsen's value[7], based on the 1 MeV Blatt data, is also an overestimate at low energy. Finally, a direct polynomial extrapolation of the Blatt data by Fukugita[8] is found to underestimate the S-factor at low energy, since it does not account for the low-energy resonance.

Based on these results, we conclude that the reaction T(^{3}He,γ)^{6}Li cannot produce sufficient ^{6}Li to explain the observed levels of ^{6}Li in primordial material. While the levels of ^{6}Li detected in some stars is debated[25], the excess has been confirmed for a few low-metallicity stars[5, 26]. We find that the reaction rates used in BBN calculations tend to either under- or over-estimate the true rate. This measurement is the first in the center-of-mass energy range relevant to BBN; thus far models have used inaccurate rates extrapolated from high-energy accelerator data. Updated BBN models based on this data will have improved fidelity. This work, and a recent study of the D(α,γ)^{6}Li reaction[6], suggest that a standard big-bang nuclear physics solution to the ^{6}Li problem is unlikely, lending weight to alternative theories such as in-situ stellar production[27] or non-Standard-Model physics[28–30].

This result is also significant in that it represents the use of HEDP to answer an open question in nuclear astrophysics, by providing the first data in the relevant energy range. As HEDP mimic conditions in stellar interiors and the universe during the big bang, a rich set of nuclear astrophysics research can be uniquely conducted at the OMEGA and National Ignition Facility[31], using this technique to study reactions at the conditions that nucleosynthesis occurred in the universe. Similar techniques can also be used to study basic nuclear science using HEDP[32–34], which further broadens the applicability of these methods.

We thank the operations crews and engineering staff at OMEGA for supporting these experiments, and E. Doeg and R. Frankel for their work processing the CR-39. This work was supported in part by the U.S. DoE (Grant No. DE-NA0001857, DE-FC52-08NA28752, DE-FG02-88ER40387, DE-NA0001837, DE-AC52-06NA25396), LLNL (No. B597367), LLE (No. 415935- G), the Fusion Science Center at the University of Rochester (No. 524431), and the National Laser Users Facility (No. DE-NA0002035). A.B.Z. acknowledges support by the National Science Foundation Graduate Research Fellowship Program under Grant No. 1122374, and gratefully acknowledges the support provided for this work by the Laboratory Directed Research and Development (LDRD) program, project number 20150717PRD2, at Los Alamos National Laboratory.

* zylstra@lanl.gov

[1] Alpher, R. A., Bethe, H. & Gamow, G. *Phys. Rev.* **73**, 803–804 (1948).
[2] Serpico, P. D. *et al. Journal of Cosmology and Astroparticle Physics* **2004**, 010 (2004).
[3] Boyd, R. N., Brune, C. R., Fuller, G. M. & Smith, C. J. *Phys. Rev. D* **82** (2010).
[4] Asplund, M., Lambert, D., Nissen, P., Primas, F. & Smith, V. *The Astrophysical Journal* **644**, 229 (2006).
[5] Fields, B. D. *Annual Review of Nuclear and Particle Science* **61**, 47–68 (2011).
[6] M. Anders *et al.* (LUNA Collaboration). *Phys. Rev. Lett.* **113**, 042501 (2014).
[7] Madsen, J. *Phys. Rev. D* **41**, 2472–2478 (1990).
[8] Fukugita, M. & Kajino, T. *Phys. Rev. D* **42**, 4251–4253 (1990).
[9] Blatt, S. L., Young, A. M., Ling, S. C., Moon, K. J. & Porterfield, C. D. *Phys. Rev.* **176**, 1147–1153 (1968).
[10] Boehly, T. *et al. Optics Communications* **133**, 495–506 (1997).
[11] Rosen, M. D. & Nuckolls, J. H. *Phys. Fluids* **22**, 1393–1396 (1979).
[12] Mack, J. *et al. Nuclear Instruments and Methods in Physics Research Section A: Accelerators, Spectrometers, Detectors and Associated Equipment* **513**, 566 – 572 (2003).
[13] Kim, Y. *et al. Phys. Plasmas* **19**, 056313 (2012).
[14] Rubery, M. *et al. Rev. Sci. Instrum.* **84**, 073504 (2013).
[15] Glebov, V. *et al. Rev. Sci. Instrum.* **77**, 10E715 (2006).
[16] Cecil, F. E., Cole, D. M., Philbin, R., Jarmie, N. & Brown, R. E. *Phys. Rev. C* **32**, 690–693 (1985).
[17] Séguin, F. *et al. Rev. Sci. Instrum.* **74**, 975–995 (2003).
[18] Brysk, H. *Plasma Physics* **15**, 611–617 (1973).
[19] Frenje, J. *et al. Rev. Sci. Instrum.* **79** (2008).
[20] Chadwick, M. *et al. Nuclear Data Sheets* **107**, 2931 – 3060 (2006). Evaluated Nuclear Data File ENDF/B-VII.0.
[21] Kühn, B., Kumpf, H., Parzhitsky, S. & Tesch, S. *Nuclear Physics A* **183**, 640–650 (1972).
[22] Munro, D. *Nuclear Fusion* **56**, 036001 (2016).
[23] Cecil, F. E., Yan, J. & Galovich, C. S. *Phys. Rev. C* **53**, 1967–1970 (1996).
[24] Tilley, D. *et al. Nuclear Physics A* **708**, 3 – 163 (2002).
[25] Lind, K., Melendez, J., Asplund, M., Collet, R. & Magic, Z. *A&A* **554**, A96 (2013).
[26] Steffen, M. *et al. arXiv* arXiv:1206.2239 [astro–ph.SR] (2012).
[27] Prantzos, N. *A&A* **542**, A67 (2012).
[28] Kusakabe, M., Kajino, T., Boyd, R. N., Yoshida, T. & Mathews, G. J. *Phys. Rev. D* **76**, 121302 (2007).
[29] Jedamzik, K. & Pospelov, M. *New Journal of Physics* **11**, 105028 (2009).
[30] Pospelov, M. & Pradler, J. *Annual Review of Nuclear and Particle Science* **60**, 539–568 (2010).
[31] Miller, G., Moses, E. & Wuest, C. *Nuclear Fusion* **44**, S228 (2004).
[32] Frenje, J. *et al. Phys. Rev. Lett.* **107**, 122502 (2011).
[33] Sayre, D. *et al. Phys. Rev. Lett.* **111**, 052501 (2013).
[34] Barbui, M. *et al. Phys. Rev. Lett.* **111**, 082502 (2013).
[35] Hale, G. M., Brown, R. E. & Jarmie, N. *Phys. Rev. Lett.* **59**, 763–766 (1987).